Ceramics International 46 (2020) 2558–2564

Contents lists available at ScienceDirect

Ceramics International

journal homepage: www.elsevier.com/locate/ceramint

Short communication

Microstructure, mechanical properties and sintering mechanism of pressureless-sintered porous Si_3N_4 ceramics with YbF_3-MgF_2 composite sintering aids

Honghui Ding, Yuan Hu, Xiaolei Li*, Zhihao Zhao, Huiming Ji

Key Laboratory for Advanced Ceramics and Machining Technology of Ministry of Education, School of Materials Science and Engineering, Tianjin University, Tianjin, 300072, PR China

ARTICLE INFO

Keywords:
Porous Si_3N_4 ceramics
Pressure sintering
YbF_3-MgF_2
Dissolution-precipitation
α-β phase transition
Mechanical properties

ABSTRACT

Porous Si_3N_4 ceramics were fabricated by pressureless sintering at 1550 °C for 2 h with YbF_3-MgF_2 composite sintering aids, systematically investigated for the effect of sintering aids addition on the microstructure and mechanical properties, further explored the formation process and sintering mechanism. The α-β phase transition rate of all samples approached 100% and MgF_2 showed a positive effect on the elongating of β-Si_3N_4 crystal grains in morphology. The apparent porosity of porous Si_3N_4 ceramics ranged from 34% to 39%. In addition, when 2.5 wt% YbF_3 was replaced by the same amount of MgF_2, the flexural strength sharply increased to 298 MPa, an increase of ~49%, while the porosity increased to 37%, an increase of ~15%. With MgF_2 content increasing from 0 to 7.5 wt%, the structure factor reached a minimum of 3.23 when MgF_2 addition was 2.5 wt%, which demonstrated unparalleled superiority in mechanical properties compared with previous studies due to a more preferred form of morphology of connected rod-like β-Si_3N_4 crystals network. Besides, our research indicated that MgF_2 addition could develop higher aspect ratio of β-Si_3N_4 grains and had obviously positive effect on the elongating characteristic of β-Si_3N_4 grains, which was related to the activation energy variation for nucleation on the different facets.

1. Introduction

As a widely-used promising structural and functional ceramics, silicon nitride (Si_3N_4) ceramics possess not only high mechanical strength and excellent thermal shock resistance, but also moderate dielectric constant as well [1,2]. Moreover, due to the fact that porous silicon nitride ceramics possess the character of both Si_3N_4 ceramics and porous ceramics, including controllable pore size distribution and customized microstructure [3], they have great potential to be used in bearings, particulate filters, high temperature structural engines, chemical metallurgical and aerospace applications [4,5].

What must be prioritized is how to maintain high porosity and excellent mechanical properties simultaneously in the research on porous Si_3N_4 ceramics [6]. The self-toughening effect of elongated β-Si_3N_4 grains, the growth of which is obtained through particle rearrangement and dissolution-precipitation mechanism in liquid phase, is conducive to the improvement of mechanical properties [7,8]. Apart from this, what should be more worthy of discussing is how to obtain a huge number of connected rod-like β-Si_3N_4 crystal grains during densification process at low cost [9,10]. In order to achieve such a super-duper microstructure, the type and amount of sintering aids and sintering process must be investigated deeply and regulated adequately to meet the demand of mechanical properties [11,12].

Sintering aids, including metal oxide, rare earth oxide, metal fluoride and rare earth fluoride, most of which possess high melting point and eutectic temperature, have been widely used and studied for the role they play during sintering process. For example, Li et al. [13] fabricated porous β-Si_3N_4 ceramics by gas pressure sintering, employing N_2 atmosphere under 1700 °C using Al_2O_3 and Y_2O_3 as sintering aids. When the addition of Si_3N_4 solid content decreased from 40 vol% to 15 vol%, the flexural strength ranged from 95 MPa to 0.1 MPa with the porosity ranging from 41% to 84%, and all the samples showed 100% phase transition rate. Zhao et al. [14] utilized Yb_2O_3–Lu_2O_3 and PMMA as composite sintering aids and pore forming agent respectively to prepare porous β-Si_3N_4 ceramics by pressureless sintering at 1750 °C for 2 h. The sample with 5 wt% Yb_2O_3 possessed a flexural strength range of 349–109 MPa and a porosity range of 15–37% with different PMMA content, and showed better mechanical properties than that

* Corresponding author.
E-mail addresses: dinghh@tju.edu.cn (H. Ding), huyuan@tju.edu.cn (Y. Hu), lxlei@tju.edu.cn (X. Li), zhaozh@tju.edu.cn (Z. Zhao), jihuiming@tju.edu.cn (H. Ji).

https://doi.org/10.1016/j.ceramint.2019.09.114
Received 2 July 2019; Received in revised form 13 August 2019; Accepted 13 September 2019
Available online 19 September 2019

with 5 wt% Lu_2O_3. However, oxide aids possess high melting temperature, which means higher sintering temperature of Si_3N_4 ceramics [15]. Based on this, Tatli et al. [16] sintered Si_3N_4 ceramics with Al_2O_3–MgO or Al_2O_3–MgF_2 composite sintering aids by Spark Plasma Sintering (SPS) and found that the sample containing Al_2O_3–MgF_2, which was sintered at 1550 °C, obtained the a maximum density of 3.15 g cm^{-3} and exhibited higher β:α ratio and superior fracture toughness than samples with Al_2O_3–MgO. This indicates that fluoride, with low melting point and glass melting temperature, shows a certain superiority in the sintering of porous Si_3N_4 ceramics. Based on previous study, we have found that compared with common oxide sintering aids, fluoride sintering aids with low melting point lead to the decrease of sintering temperature, and Yb ions lead to the decrease of free energy upon nucleation, which is in favor of α-β phase transition and the improvement of mechanical properties of Si_3N_4 ceramics significantly [17,18]. And MgF_2, with a melting point of 1261 °C, in which the network terminating effect of fluorine leads to the decrease of glass transition point and glass melting point, offering more adequate time for the transition from α phase and β phase and liquid phases to be formed at low temperature [19].

Herein, we fabricated porous Si_3N_4 ceramics using α-Si_3N_4 as raw materials and YbF_3-MgF_2 as non-oxide sintering aids by pressureless sintering at relatively low temperature, reducing the production cost compared with other sintering process. The effect of sintering aids addition on the microstructure and mechanical properties, together with the formation process and sintering mechanism of porous Si_3N_4 ceramics were investigated in detail. In all samples, almost all α-Si_3N_4 completely changed into β-Si_3N_4. Additionally, when YbF_3 was replaced with the equal amount of MgF_2, both the flexural strength and the porosity were increased crucially. And the minimum value of structure factor reached 3.23, which was pretty low compared with previous study.

2. Experimental

2.1. Raw materials

Table 1 shows the function, purity and manufacture of the raw materials employed in this experiment.

2.2. Fabrication procedures

In this work, porous Si_3N_4 ceramics were prepared by pressureless sintering at relatively low temperature and the codes and composition are shown in Table 2.

Starting powders were Si_3N_4 (α ratio > 95.5%), YbF_3 and MgF_2. Firstly, the starting powders were mixed with 0.5 wt% Polyvinyl Butyral as a binder in ethanol to form a slurry. After ball milling and drying at 90 °C, the obtained powders were sieved through a 120-mesh sieve. Then, the dry press processing was conducted under 20 MPa, which was followed by isostatic pressing under 200 MPa. Finally, the green body was sintered at 600 °C to exclude binders, and heated at 1550 °C for 2 h employing N_2 atmosphere by pressureless sintering to form the final sintered bodies.

Table 2
Codes and compositions of the porous Si_3N_4 ceramics.

Codes	compositions
S*	10 wt%YbF_3
SMg0	7.5 wt%YbF_3 + 0 wt% MgF_2
SMg2.5	7.5 wt%YbF_3 + 2.5 wt% MgF_2
SMg5	7.5 wt%YbF_3 + 5 wt% MgF_2
SMg7.5	7.5 wt%YbF_3 + 7.5 wt% MgF_2

2.3. Characterizations

The particle size of starting powders was determined by eceshi with Laser Particle Size Analyzer (Mastersizer 2000, Britain). The morphology was observed using scanning electron microscope (SEM, S4800, Hitachi, Japan). The porosity of Si_3N_4 ceramics was measured through the Archimedes Method. The crystalline phase was identified using X–ray diffractometer (XRD, Rigaku D/Max 2500, Japan). The grain size was determined from SEM images by measuring diameter and length of 200 grains using particle size measurement software. Besides, we take the average of grain sizes and have statistics on frequency distribution of porous Si_3N_4 grains. The element type and content were analyzed using Energy Dispersive Spectrometer (EDS, JSM-7800F, Japan).

The Si_3N_4 phase content (β%, wt.%) was determined from the characteristic diffraction peak intensities of (101) planes of β-Si_3N_4 ($I_{\beta\,(101)}$) and (201) planes of α-Si_3N_4 ($I_{\alpha\,(201)}$) in XRD patterns according to the Gazzara and Messier method, the calculation formula is as follows [20,21]:

$$\beta(\%) = \left[1.4434\left(\frac{I_{\beta(101)}}{I_{\beta(101)} + I_{\alpha(201)}}\right) - 0.4434\left(\frac{I_{\beta(101)}}{I_{\beta(101)} + I_{\alpha(201)}}\right)^2\right] \times 100 \quad (1)$$

The three-point bending method was performed on test bars of 3 mm × 4 mm × 30 mm to measure the flexural strength (σ) in a universal testing machine (Jinshengxin Test Instrument Co. Ltd., Beijing, China). Single-edge notched beam (SEBN) was used to measure the fracture toughness (K_{IC}) of specimens (XWW, Chengde Hengtong Test Instrument Co. Ltd., Chengde, China).

3. Results and discussion

3.1. The phase transition and microstructural characteristics of porous Si_3N_4 ceramics

As is shown in Fig. 1 of XRD pattern of the samples sintered at 1550 °C, β-Si_3N_4 is the major existing form of Si_3N_4 ceramics, while the amount of α-Si_3N_4 is less than 5% of all the samples calculated by characteristic diffraction peak intensities. Besides, no Mg-containing phase is found in XRD pattern, which is probably due to the weak diffraction peak intensity or the forming of amorphous state. Meanwhile, $Yb_4Si_2N_2O_7$ is detected in SMg2.5 and SMg5, which possesses preferable high-temperature stability than $Yb_2Si_3O_4N_3$ in contrast sample S* [22]. The 100% phase transition of SMg2.5 and SMg5 profits

Table 1
Raw materials and reagents.

Raw materials	Function	Purity	Particle size	Manufacture
Si_3N_4 powder	Raw powders	α ratio > 95.5%	0.5 μm	UBE Industries Co., Ltd., Japan
YbF_3	Sintering aid	≥99.7%	2.7 μm	Xinzhen Rare Earth New Materials Co., Ldt., Jiangxi, China
MgF_2	Sintering aid	≥99.7%	13.4 μm	Shanghai Aladdin Bio-Chem Technology Co., Ldt., Shanghai, China
Ethanol	Grinding media	≥99.7%	\	Yuanli chemical Co., Ltd., Tianjin, China
Polyvinyl Butyral	Binder	≥99.7%	607.6 μm	Solutia Co., Ltd., America
PEG 600	surfactant	≥99.7%	\	Guangfu Fine Chemical Co., Ltd., Tian, China

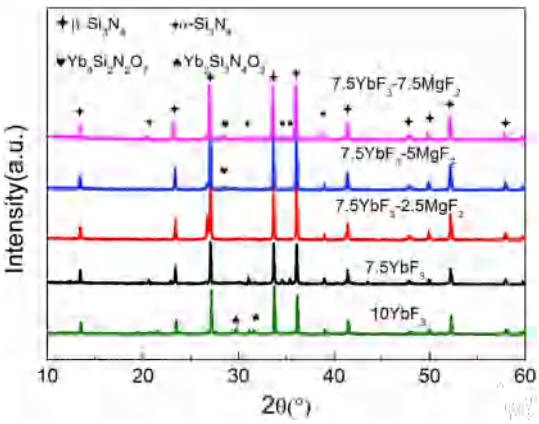

Fig. 1. XRD pattern of porous Si_3N_4 ceramics with different sintering aids addition.

from lower-temperature liquid phase system during the dissolution-precipitation process. According to the phase diagram of the YbF_3-MgF_2 system, the eutectic point is 967 °C consisting of about 88 wt% YbF_3 and 12 wt% MgF_2 [23]. Appropriate content of YbF_3-MgF_2 composite sintering aids could lower the liquid generating temperature, reduce the viscosity of liquid phase and increase material diffusion coefficient, thus enabling α-Si_3N_4 grains to be more completely wetted and adequately dissolved, reducing the energy for nucleation and growth and then precipitating out radioactive elongate β-Si_3N_4 grains. And with the MgF_2 addition increasing, the composition deviates from the eutectic point, which leads to the incomplete α-β phase transition of SMg7.5.

Fig. 2(a)-(e) exhibit SEM micrographs of samples S*, SMg0, SMg2.5, SMg5, SMg7.5, respectively. All the samples possess elongated shapes to form an excellent microstructure of interconnected network of β-Si_3N_4 grains, which is conducive to the improvement of mechanical properties. As can be seen from the EDS analysis results in Fig. 2(f), silicon, nitrogen, oxygen and ytterbium, magnesium and fluorine are the main elements in SMg2.5, which account for separately as 57.73 wt%, 37.73 wt%, 1.07 wt %, 2.55 wt%, 0.26 wt and 0.67 wt%. And on the one hand, as a glass network disrupter, fluorine could reduce glass melting temperature and glass transition temperature so that using MgF_2 as a sintering aid could provide more sufficient time for the precipitation of β-phase from liquid phase [24], making grains grow more adequately. Besides, on the other hand, the fluorine content of all samples is below 1 wt%, which is far too low to damage to the high temperature mechanical properties of porous Si_3N_4 ceramics. On the purpose of characterizing grain growth situation more expediently and visually, histogram of frequency distribution of porous Si_3N_4 grains with different sintering aids are combined to carry out analysis as can be seen from Fig. 3 and the measuring results of average sizes are listed in Table 3. For sample S* in Fig. 2(a), it can be observed apparently that β-Si_3N_4 grains are not as elongated as those in other samples. Additionally, it can also be proved from the distribution of length and aspect ratio in Fig. 3, which present a distinct offset direction to smaller numerical value. The average length is 1.65 μm and average aspect ratio is 6.35 for sample S*, while the average length is 2.67 μm and average aspect ratio is 8.60 for sample SMg2.5. When we add a small amount of MgF_2 to replace part of YbF_3 as can be seen from contrast sample S* and SMg2.5, the β-Si_3N_4 grains can have a better connection with each other and porous Si_3N_4 ceramics can possess more excellent microstructure. Accordingly, the mechanical properties of Si_3N_4 are profoundly enhanced. From Fig. 3(a)–(b), as more MgF_2 content is gradually added, more liquid phase is produced, the number value of sizes is increasing and the dispersity of large elongated grains represents a trend of rise. The average length of the samples increases, ranging from 2.28 μm to 3.52 μm and the average aspect ratio of the samples increases, ranging from 8.25 to 11.11, which represents the elongating effect of MgF_2 on β-Si_3N_4 grains.

3.2. Mechanical properties of porous Si_3N_4 ceramics

Fig. 4 shows porosity, flexural strength and structure factor of porous Si_3N_4 ceramics with different sintering aids addition. Similarly, taking the same weight of sintering aids samples S* and SMg2.5 for contrast, when the same amount of MgF_2 works as a substitute for part of YbF_3, the flexural strength sharply rises to 298 MPa, while the porosity also rises to 37%, compared with the sample contain 10 wt% YbF_3, which possesses flexural strength of 200 MPa and porosity of 33%. To evaluate the relationship between porosity and corresponding strength at room temperature, the structure factor is calculated, which is one of the most important mechanical indexes of Si_3N_4 ceramics, and the equation is as follows [25–27]:

$$\sigma = \sigma_0 \exp(-bp) \tag{2}$$

where σ denotes the flexural strength, b denotes the structure factor and p denotes the porosity, σ_0 denotes the theoretical strength of dense Si_3N_4 ceramics and is 1000 MPa, which is the flexural strength when the porosity is 0.

With the porosity unchanged, Si_3N_4 ceramics with smaller structure factor have a better performance on strength. As MgF_2 addition increases, the structure factor initially decreases, ranging from 4.16 to 3.23, reaches the minimum value in SMg2.5 and then increases to 3.41 by inches. Thus, it is concluded that SMg2.5 possesses the best strength in the same conditions of porosity. The addition of a small amount of MgF_2 lower the melting point, provide much liquid phase and appropriate duration to form an interconnected structure at relatively low temperature. It is widely acknowledged that the pores and defects damage the mechanical properties, whereas the increase of density generally results in the improvement of strength. Nevertheless, the samples can still possess super-duper mechanical strength, due to the contribution of the unique interlocking microstructure of β-Si_3N_4 grains with adequate aspect ratio, where the grain bridging and pull-out mechanism perform a significant function [28]. As MgF_2 content increases from 2.5 wt% to 7.5 wt%, the variation of structure factor is much smaller compared with that from 0 to 2.5 wt%. When MgF_2 content is 5 wt%, the sample possesses the lowest porosity of 34% and the highest flexural strength of 317 MPa compared with other Mg-containing samples owing to the more complete densification process. In essence, as MgF_2 content increases from 0 to 5 wt%, the amount of liquid phase increases, which gradually fills the pores and improve the contact between grains, leading to the decrease of porosity and higher level of densification. However, when MgF_2 content reaches 7.5 wt%, excess MgF_2 favors the aggregation of glass phase at grain boundary, which hinders diffusion and grain-boundary movement, thus doing harm to densification process, grain growth and mechanical properties. Therefore, for SMg7.5, the MgF_2 content of which is 7.5 wt%, the flexural strength decreases, which is related the increase of porosity, the excess glass phase and the condition of β phase. Besides, Table 2 reveals that as MgF_2 content increases from 0 wt% to 7.5 wt%, the fracture toughness of Si_3N_4 samples first increases and then decreases, reaches maximum value at 4.35 MPa•$m^{1/2}$ achieved by sample SMg5 with a high aspect ratio and elongated interconnected β-Si_3N_4 grains. Additionally, the superior mechanical strength of porous Si_3N_4 ceramics benefits from the fact that YbF_3-MgF_2 composite sintering aids with low eutectic point contribute to reducing the melting point and accelerating the generation of β-Si_3N_4 crystal grains by providing much liquid phase at relatively low temperature.

3.3. The formation process and sintering mechanism of porous Si_3N_4 ceramics

The schematic diagram of the formation mechanism of porous Si_3N_4 is shown in Fig. 5(a)-(e). In many previous researches, the sintering aids encourage liquid phase to be generated during the sintering procedure.

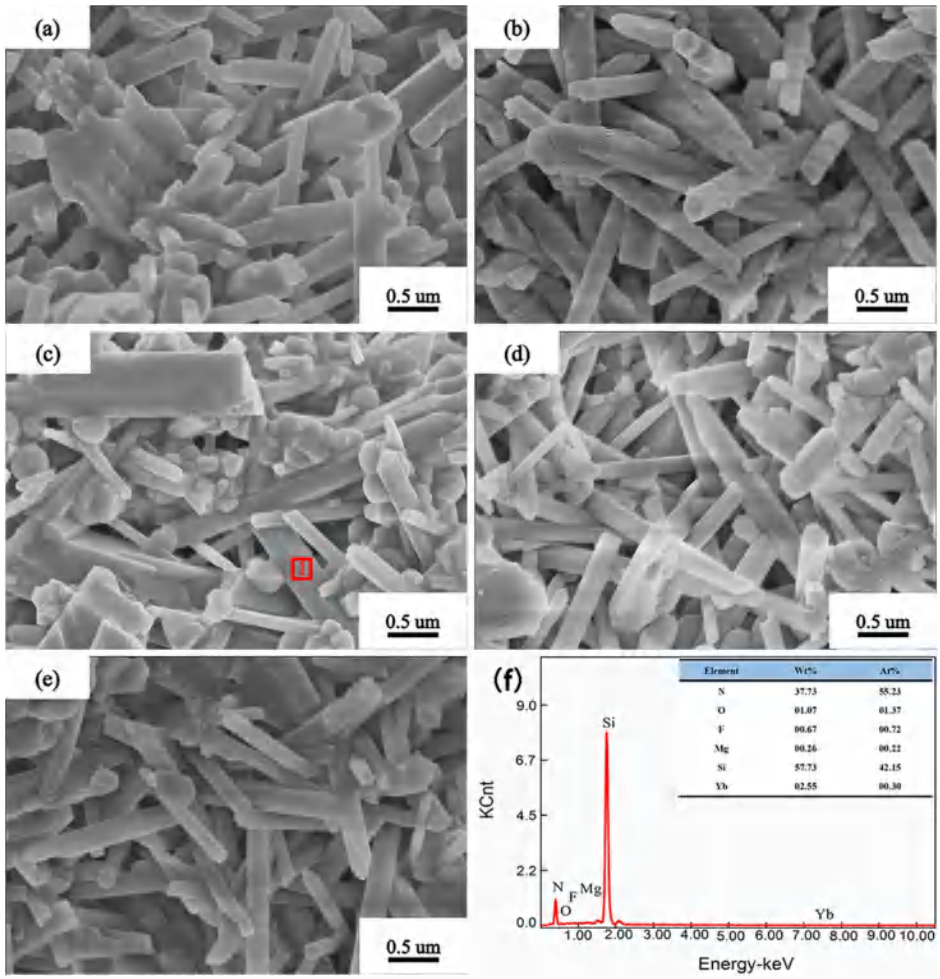

Fig. 2. SEM micrographs of porous Si_3N_4 ceramics with different sintering aids addition: (a) S*, (b) SMg0, (c) SMg2.5, (d) SMg5, (e) SMg7.5; (f) EDS patterns of area 1 in (c).

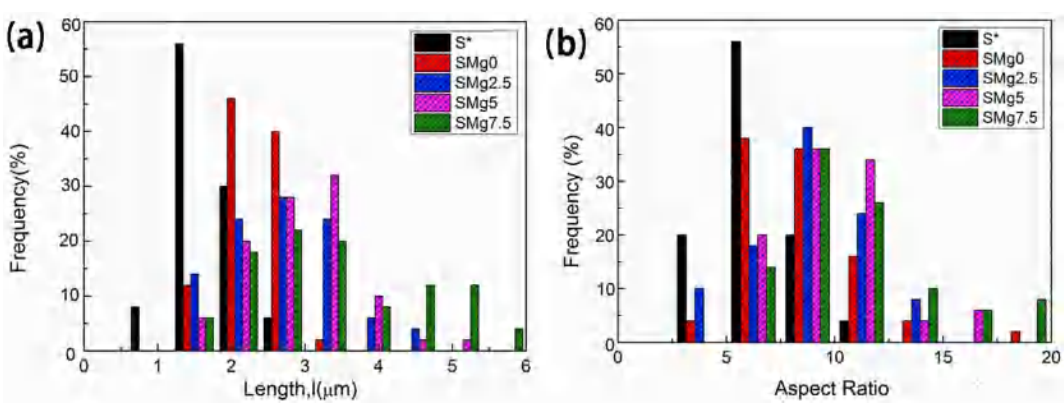

Fig. 3. Frequency distribution of porous Si_3N_4 grains with different addition of sintering aids: (a) histogram of grain length, (b) histogram of aspect ratio.

Table 3
β%, average sizes and K_{IC} of the samples with different sintering aids addition.

Compositions	S*	SMg0	SMg2.5	SMg5	SMg7.5
β%	98	96	100	100	98
Average length(μm)	1.65	2.28	2.67	2.89	3.52
Average width(μm)	0.27	0.30	0.34	0.31	0.41
Average aspect ratio	6.35	8.25	8.60	10.40	11.11
K_{IC}(MPa•m$^{1/2}$)	3.47 ± 0.68	3.58 ± 0.28	3.78 ± 0.08	4.35 ± 0.36	4.09 ± 0.06

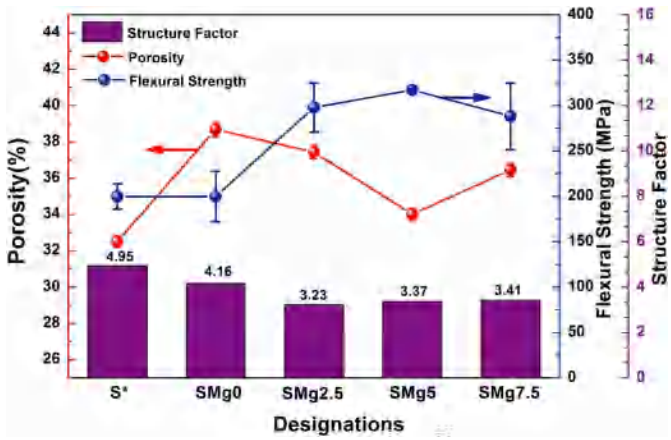

Fig. 4. Porosity, flexural strength and structure factor of porous Si_3N_4 ceramics with different sintering aids addition.

As we used YbF_3-MgF_2 as sintering aids which have low glass melting points, liquid phase viscosity is significantly reduced [29], thereby sufficient liquid phase is accordingly generated at relatively lower temperature as can be seen from Fig. 5(b). Adequate liquid phase guarantees that α-Si_3N_4 particles can be completely wetted, thus promoting the process of particle rearrangement and the formation of fibrous β- Si_3N_4 via uniform nucleation mechanism [18].

As shown in Fig. 5(c), when the phase transition temperature is reached, α-β phase transition initiates and β-Si_3N_4 crystal grains are formed through dissolution-precipitation mechanism. During the process, the growth of β-Si_3N_4 crystal grains is diffusion-controlled through Ostwald ripening [30]. Due to the addition of fluoride, the lower viscosity [29] is beneficial for diffusion and mass transmission according to Stokes-Einstein equation as follows:

$$\eta = \frac{kT}{6\pi rD} \tag{3}$$

where η denotes liquid phase viscosity, r denotes the radius of diffusing species, D denotes diffusion constant, k denotes the Boltzmann constant, T denotes the thermodynamic temperature, respectively. With lower liquid phase viscosity, the resulting increasing diffusion constant could enable β-Si_3N_4 crystal grains to grow more efficiently with high quality. As sintering temperature increases, the solid particles that dispersed in the liquid phase are rearranged. Part of the solid particles dissolve and then precipitate out elongated β-Si_3N_4 crystals (Fig. 5(d)). Besides, most SiF_4, which is the reaction product of SiO_2 and fluoride sintering aids, would get out of the system. With β-Si_3N_4 crystals growing, the fibrous β-Si_3N_4 connect to and cross with each other to form a cross-linked network structure [31,32]. At the end of the sintering procedure, all of the α-Si_3N_4 are transformed into well-

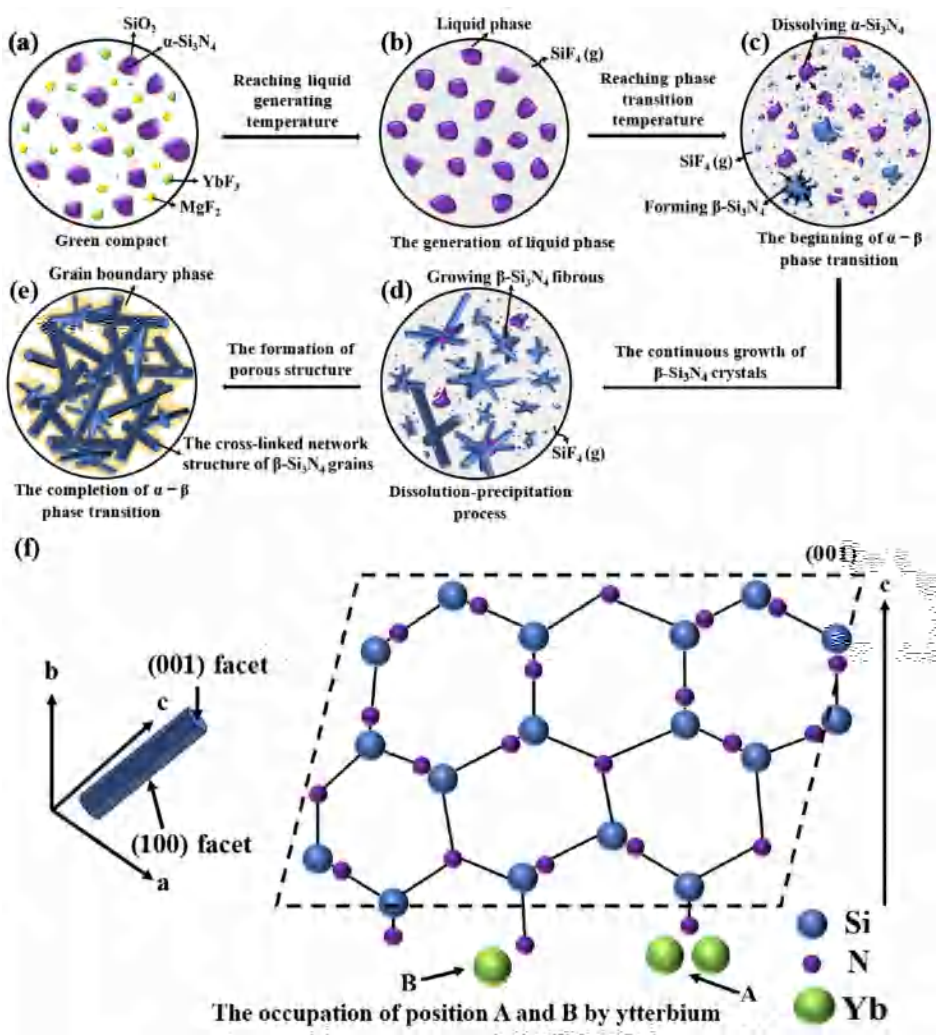

Fig. 5. (a)–(g) The schematic diagram of the formation process of β-Si_3N_4 crystal network; (f)The effect of Yb atoms on the network structure of β-Si_3N_4 crystal.

structured, radioactive elongated β-Si_3N_4 crystals, which are interlocked and bonded with each other by the grain-boundary phase (Fig. 5(e)), thus enabling Si_3N_4 ceramics to maintain excellent mechanical properties while possessing a porous microstructure.

It is noteworthy that with a small radius, Yb atoms can bond to two atomic positions, A and B, along the Si_3N_4 prismatic plane [33] (Fig. 5(f)), leading to a reduction in interfacial energy increased upon the nucleation, that is, the lowest activation energy, which would be comparable to diffusion activation energy [17], and resulting in a more complete α-β phase transition and a more preferred form of morphology of cross-linked β-Si_3N_4 crystals. The fluorine in YbF_3-MgF_2 composite sintering aids can disrupt the network of glass phase by substituting for bridging oxygen to form Si–F bond [34], which results in the decrease of both glass melting point and glass transitions point [19], offering more adequate time for the completion of transition from α to β. Based on the research of predecessors, it is an essential feature for β-Si_3N_4 crystal grains to show elongated shape, which is originated from much higher activation energy for nucleation on the (100) facet than on the (001) facet [35], which is equal to higher grain growth rate along c axis. In this study, with the increase of MgF_2 content, ample liquid phase can be generated at lower temperature, allowing a more complete growth and development of β-Si_3N_4 crystal grains, which can be proved from the increasing average length and width in Table 3. On this basis, the addition of MgF_2 makes the essential feature mentioned above much clearer, which means grains could grow faster along c axis and the rate of increase in length is much greater than that in width, leading to the increase of aspect ratio and the elongating of β-Si_3N_4 crystal grains. Apart from this, with a eutectic point of 967 °C [23], which is pretty low in comparison with other aids, the YbF_3-MgF_2 composite sintering aids reduce the glass transition temperature (Tg) and viscosities of the glasses [35], leading to the generation of more liquid phase at lower temperature, thus β-Si_3N_4 grains are able to grow better in the ample liquid phase, which is consistent with the result of microstructure and mechanical property analysis.

4. Conclusions

Low temperature pressureless sintering porous Si_3N_4 ceramics were fabricated at 1550 °C for 2 h with low eutectic point YbF_3-MgF_2 as composite sintering aids. α-Si_3N_4 could completely precipitate in form of β phase with appropriate phase transition duration from adequate low temperature liquid phase through dissolution-precipitation mechanism. The composite sintering aids YbF_3-MgF_2 play a crucial role in the fabrication of radioactive elongated β- Si_3N_4 crystals to obtain porous Si_3N_4 ceramics with optimized microstructure and mechanical performance. All samples represented nearly 100% α-β phase transition rate. The flexural strength and porosity of the specimen containing 2.5 wt% MgF_2 and 7.5 wt% YbF_3 reached 298 MPa and 37%, respectively, which were increased by ~49% and ~15% compared to the values of the counterparts with 10 wt% YbF_3 as sintering aids, and the structure factor reached minimum value of 3.23, which showed obvious advantages in mechanical properties. Apart from this, the addition of MgF_2 could make β-Si_3N_4 grains grow longer along c axis, develop higher aspect ratio of β-Si_3N_4 grains and have obviously positive effect on the elongating characteristic of β-Si_3N_4 grains, resulting in the cross-linked network structure and super-duper mechanical properties of Si_3N_4 ceramics.

Acknowledgments

We acknowledge the funding supports from National Natural Science Foundation of China (Grant. No.: 51202157), Tianjin Research Program of Application Foundation and Advanced Technology (Grant. No.: 14JCQNJC02800), and Independent Innovation Foundation of Tianjin University.

References

[1] H.J. Wang, J.L. Yu, J. Zhang, D.H. Zhang, Preparation and properties of pressureless-sintered porous Si_3N_4, J. Mater. Sci. 45 (2010) 3671–3676.
[2] T.T. Liu, C.F. Jiang, W. Guo, Effect of CeO_2 on low temperature pressureless sintering of porous Si_3N_4 ceramics, J. Rare Earths 35 (2017) 172–176.
[3] X.M. Li, R. Li, X.T. Zhu, Y.L. Zhu, G.N. Ren, L. Zhang, Properties of large-sized porous Si_3N_4 ceramic tubes fabricated by carbothermal reduction of diatomite preforms, Ceram. Int. 43 (2017) 10559–10565.
[4] S. Yin, S.C. Jiang, L.M. Pan, C. Liu, Y.B. Feng, T. Qiu, Preparation, mechanical and thermal properties of Si_3N_4 ceramics by gelcasting using low-toxic DMAA gelling system and gas pressure sintering, Ceram. Int. 44 (2018) 22412–22420.
[5] J.H. Dai, J.B. Li, Y.J. Chen, L. Yang, Effect of the residual phases in β-Si_3N_4 seed on the mechanical properties of self-reinforced Si_3N_4 ceramics, J. Eur. Ceram. Soc. 23 (2003) 1543–1547.
[6] A. Parsi, F. Golestanifard, S.M. Mirkazemi, The effect of gelcasting parameters on microstructural optimization of porous Si_3N_4 ceramics, Ceram. Int. 45 (2019) 9719–9725.
[7] H. Klemm, Silicon nitride for high-temperature applications, J. Am. Ceram. Soc. 93 (2010) 1501–1522.
[8] C. Kawai, A. Yamakawa, Effect of porosity and microstructure on the strength of Si_3N_4: designed microstructure for high strength, high thermal shock resistance, and facile machining, J. Am. Ceram. Soc. 80 (1997) 2705–2708.
[9] L. Xie, D.X. Yao, Y.F. Xia, J.W. Yin, H.Q. Liang, K.H. Zuo, Y.P. Zeng, High porosity Ca-α-SiAlON ceramics with rod-like grains fabricated by freeze casting and pressureless sintering, J. Eur. Ceram. Soc. 39 (2019) 2036–2041.
[10] Z.H. Wang, B. Bai, X.S. Ning, Effect of rare earth additives on properties of silicon nitride ceramics, Adv. Appl. Ceram. 113 (2014) 173–177.
[11] H.Q. Liang, Y.P. Zeng, K.H. Zuo, D.X. Yao, J.W. Yin, Mechanical properties and thermal conductivity of Si_3N_4 ceramics with YF_3 and MgO as sintering additives, Ceram. Int. 42 (2016) 15679–15686.
[12] M. Kitayama, K. Hirao, K. Watari, M. Toriyama, S. Kanzaki, Thermal conductivity of β-Si_3N_4: III, effect of rare- earth (RE = La, Nd, Gd, Y, Yb, and Sc) oxide additives, J. Am. Ceram. Soc. 84 (2001) 353–358.
[13] L. Li, Q.G. Li, J. Hong, M.Y. Sun, J. Zhang, S.M. Dong, Effect of Si_3N_4 solid contents on mechanical and dielectric properties of porous Si_3N_4 ceramics through freeze-drying, J. Alloy. Comp. 732 (2018) 136–140.
[14] Z.H. Zhao, X.L. Li, D. Su, M.J. Wu, H.M. Ji, Microstructure and properties of pressureless-sintered porous Si_3N_4 using PMMA as pore-forming agent, Integr. Ferroelectr. 171 (2016) 46–51.
[15] H. Hayashi, K. Hirao, M. Toriyama, M. Kanzaki, $MgSiN_2$ addition as a means of increasing the thermal conductivity of β-silicon nitride, J. Am. Ceram. Soc. 84 (2001) 3060–3062.
[16] Z. Tatlı, F. Çalışkan, J. Butler, C. Crowley, S. Hampshire, SPS sintering of silicon nitride with fluoride additive, Ceram. Int. 40 (2014) 1399–1404.
[17] M. Kitayama, K. Hirao, S. Kanzaki, Effect of rare earth oxide additives on the phase transformation rates of Si_3N_4, J. Am. Ceram. Soc. 89 (2006) 2612–2618.
[18] H.H. Ding, Z.H. Zhao, T. Qi, X.L. Li, H.M. Ji, High α-β phase transition and properties of YbF_3-added porous Si_3N_4 ceramics obtained by low temperature pressureless sintering, Int. J. Refract. Metals Hard Mater. 78 (2019) 131–137.
[19] F. Hu, L. Zhao, Z.P. Xie, Silicon nitride ceramics with high thermal conductivity and excellent mechanical properties fabricated with MgF_2 sintering aid and post-sintering heat treatment, J. Ceram. Sci. Tech. 7 (2016) 423–428.
[20] C.P. Gazzara, D.R. Messier, Determination of phase content of Si_3N_4 by X-ray diffraction analysis, Am. Ceram. Soc. Bull. 56 (1977) 777–780.
[21] L. Fan, M. Zhou, H.J. Wang, Z.Q. Shi, X.F. Lu, C. Wang, Low-temperature preparation of β-Si_3N_4 porous ceramics with a small amount of Li_2O-Y_2O_3, J. Am. Ceram. Soc. 97 (2014) 1371–1374.
[22] Y. Liu, J.B. Li, Y.J. Chen, J.H. Dai, Secondary crystalline phases and mechanical properties of heat-treated Si_3N_4, Mater. Sci. Eng. A363 (2003) 93–98.
[23] L.A. Olkhovaya, P.P. Fedorov, D.D. Ikrami, B.P. Sobolev, Phase diagrams of MgF_2-(Y, Ln) F_3 systems, J. Therm. Anal. 15 (1979) 355–360.
[24] A.R. Hanifi, A. Genson, M.J. Pomeroy, S. Hampshire, Oxyfluoronitride glasses with high elastic modulus and low glass transition temperatures, J. Am. Ceram. Soc. 92 (2009) 1141–1144.
[25] R.L. Coble, W.D. Kingery, Effect of porosity on physical properties of sintered alumina, J. Am. Ceram. Soc. 39 (1956) 377–385.
[26] C. Kawai, A. Yamakawa, Effect of porosity and microstructure on the strength of Si_3N_4: designed microstructure for high strength, high thermal shock resistance, and facile machining, J. Am. Ceram. Soc. 80 (1997) 2705–2708.
[27] J. Zhou, J.P. Fan, G.L. Sun, J.Y. Zhang, X.M. Liu, D.H. Zhang, H.J. Wang, Preparation and properties of porous silicon nitride ceramics with uniform spherical pores by improved pore-forming agent method, J. Alloy. Comp. 632 (2015) 655–660.
[28] H. Park, H.E. Kim, K. Niihara, Microstructural evolution and mechanical properties

of Si_3N_4 with Yb_2O_3 as a sintering additive, J. Am. Ceram. Soc. 80 (1997) 750–756.
[29] A. Stamboulis, R.G. Hill, R.V. Law, Characterization of the structure of calcium alumino-silicate and calcium fluoro-alumino-silicate glasses by magic angle spinning nuclear magnetic resonance (MAS-NMR), J. Non-Cryst. Solids 333 (2004) 101–107.
[30] J. Yang, J.F. Yang, S.Y. Shan, J.Q. Gao, Effect of sintering additives on microstructure and mechanical properties of porous silicon nitride ceramics, J. Am. Ceram. Soc. 89 (2006) 3843–3845.
[31] Z.W. Luo, H.Z. Liang, C.C. Qin, J. Zhang, T.Y. Liu, A.X. Lu, Sintering behavior, microstructures and mechanical properties of porous CaO-Al_2O_3-SiO_2-Si_3N_4 glass-ceramics, J. Alloy. Comp. 773 (2019) 71–77.
[32] B. Li, P. Jiang, M.W. Yan, Y. Li, X.M. Hou, J.H. Chen, Characterization and properties of rapid fabrication of network porous Si_3N_4 ceramics, J. Alloy. Comp. 709 (2017) 717–723.
[33] A. Ziegler, J.C. Idrobo, M.K. Cinibulk, C. Kisielowski, N.D. Browning, R.O. Ritchie, Interface structure and atomic bonding characteristics in silicon nitride ceramics, Science 306 (2004) 1768–1770.
[34] F. Çalışkan, Z. Tatlı, A. Genson, S. Hampshire, Pressureless sintering of β-SiAlON ceramic compositions using fluorine and oxide additive system, J. Eur. Ceram. Soc. 32 (2012) 1337–1342.
[35] W.K. Li, D.Y. Chen, B.L. Zhang, H.R. Zhuang, W.L. Li, Effect of rare-earth oxide additives on the morphology of combustion synthesized rod-like β-Si_3N_4 crystals, Mater. Lett. 58 (2014) 2322–2325.